Thermal transport in a dielectric T-shaped quantum wire

Ping Yang,[1,2] Qing-feng Sun,[2,3] Hong Guo,[2] and Bambi Hu[1,4]
[1]*Department of Physics, Centre for Nonlinear Studies, and The Beijing-Hong Kong-Singapore Joint Centre for Nonlinear and Complex Systems (Hong Kong), Hong Kong Baptist University, Kowloon Tong, Hong Kong, China*
[2]*Center for the Physics of Materials and Department of Physics, McGill University, Montreal, Quebec, Canada H3A 2T8*
[3]*Institute of Physics, Chinese Academy of Sciences, Beijing 100080, China*
[4]*Department of Physics, University of Houston, Houston, Texas 77204-5005, USA*
(Received 3 August 2006; revised manuscript received 3 May 2007; published 19 June 2007)

We investigate the thermal transport in a special ballistic system, the dielectric T-shaped quantum wire. It is found that the transmission coefficient of phonons exhibits the oscillation behavior similar to that of electrons. Due to the wide energy range involved in thermal transport, thermal conductance changes smoothly with temperature, which is different from the electrical conductance. We find that thermal conductance is a monotonic function of temperature at any system. In the low temperature limit, thermal conductance tends to $\frac{\pi^2 k_B^2 T}{3h}$ against all system parameters, even though the transmission coefficient is not unity.

DOI: 10.1103/PhysRevB.75.235319 PACS number(s): 66.70.+f, 44.10.+i, 63.22.+m, 63.20.Dj

I. INTRODUCTION

For recent years, phonon transport in mesoscopic system at low temperature has been paid much attention both theoretically,[1–7] and experimentally.[8–11] Similar to the related case of electrical conduction in the mesoscopic regime,[12] for a perfect sample, we can view the finite resistance for phonon propagation as coming from the nonideal connection between the thermal reservoir and the one-dimensional sample. At very low temperatures, due to phonon wavelength comparable to the geometrical size of the system, the universal quantum of thermal conductance $G_0=\frac{\pi^2 k_B^2 T}{3h}$ has been predicated theoretically in a one-dimensional sample with the perfect contact to two thermal reservoirs[1,2] and observed experimentally by Schwab *et al.*[8] Different from classical situation, thermal energy in the quantum regime is carried by a set of discrete phonon energy subbands or vibrational modes with a finite cutoff frequency in the one-dimensional system due to transverse confinement. Because interaction between the discrete vibrational modes could not be considered in the temperature less than 1 K, phonons transport ballistically in a one-dimensional sample without energy loss and each mode contributes G_0 to the total thermal conductance G: a perfect sample has $G=N_0G_0$ which is a finite number, where N_0 is the number of modes with zero cutoff frequency, i.e., the massless modes. When temperature becomes higher, the higher energy modes with nonzero cutoff frequencies will open up and thus thermal conductance will increase over the universal value. Thermal conductance shows a dependence on the intrinsic properties and on the geometrical features of sample through the cutoff frequencies.[1,7,13]

In mesoscopic regime, the influence of geometrical structure was most clearly demonstrated in electron charge transport.[14,15] Electrons transmitting through a one-dimensional wire with a side stub, i.e., the T-shaped junction, have been investigated by several groups both experimentally and theoretically.[16,17] Charge transport through such a device reveals interesting features of electrical conductance, such as the observed conductance plateaus, resonances, zero transmission at certain values of the side-stub length, etc. More recently, the investigations were carried out in both charge and heat transports through a curve wire and a diffusive metallic wire coupled with a superconducting wire, i.e., the T-shaped junction.[18,19]

In this paper, we investigate the thermal transport properties in a special ballistic system, the dielectric T-shaped quantum wire shown in Fig. 1. As we will show, although the geometrical structure in Fig. 1. is simple, rather complicated phonon transmission does appear due to interference effect. For instance, a slight change of the structure size will be possible to affect the phonon propagation and thereby thermal conductance. Comparing to electron transport, we find that the phonon transmission coefficient has an oscillation behavior similar to that of electrons. However, thermal conductance increases monotonically with temperature. This result is different from electrical conductance which is not a monotonic function of both temperature and bias.[20,21] In the low temperature limit, thermal conductance tends to $\frac{\pi^2 k_B^2 T}{3h}$ even though transmission coefficient $\tilde{T}_m(\omega)\equiv 1$. This behavior is different from classical thermal conductance, in which it is an extensive quantity and is proportional to the width of terminal wire.

The rest of the paper is organized as follows. In Sec. II, the device's model is presented and the formula of the transmission coefficient is derived. In Sec. III, we numerically investigate the transmission coefficient. The thermal conduc-

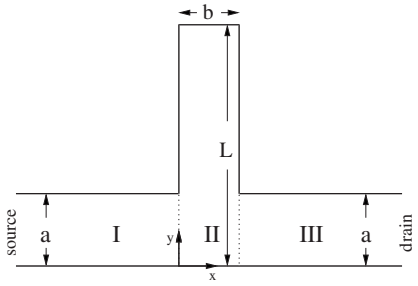

FIG. 1. Schematic diagram for the T-shaped wire.

tance is studied in the Sec. IV. Finally, conclusions are summarized in Sec. V.

II. MODEL AND FORMULATION

The dielectric T-shaped quantum wire is considered to be a two-dimensional system in the x-y plane, shown in Fig. 1. It has two long and perfect leads with uniform width **a**, which join a rectangular stub with width **b** and length **L**. We divide the structure into three regions: the left lead is region I, the right lead region III, and the scattering region is region II which includes the side stub. The other ends of leads are connected separately to two thermal reservoirs with a temperature bias $T_L > T_R$; here, T is the temperature of the left (L) and right (R) reservoirs. The reservoirs are at thermal equilibrium with phonon distributions in the Bose-Einstein form, i.e., $\eta(\omega)=(e^{\hbar\omega/k_BT}-1)^{-1}$. We assume "reflectionless" contacts between the leads and the reservoirs: any wave going into a reservoir disappears inside the reservoir without being reflected back to the leads. This is a reasonable assumption because reservoirs are far away and we are not interested in them. At low temperature, phonon-phonon interactions between different vibrational modes can be safely neglected. In this way, the leads act as phonon waveguides. Assuming that an incident wave comes from the left lead (region I), it then enters the scattering region II where it suffers elastic scattering due to the different geometrical shape, and finally, the wave partially transmits to the right lead (region III) and partially reflects back to the left lead.

In the low temperature, phonon wavelength is generally over a few hundreds of angstroms which can be greater than the width of the side stub **b** and width of the wire **a**. Such a wavelength is certainly much greater than any microscopic length such as the atomic bond length. Therefore, the scalar model of continuum medium theory can be used to describe the wave propagation. According to this theory, the displacement field $u(x,y)$ satisfies the wave equation[22]

$$v^2\nabla^2 u(x,y) + \omega^2 u(x,y) = 0, \tag{1}$$

where ω is the frequency of wave and v is the sound velocity. The structure surface provides free boundary conditions so that $\frac{\partial u}{\partial n}=0$, where n is the unit vector perpendicular to the surface.

In terms of Eq. (1), the solutions in regions I, II, and III are written as follows:

$$u^{(\mathrm{I})} = \Psi_m(y)e^{ik_m x} + \sum_{n=0}^{\infty} r_{nm}\Psi_n(y)e^{-ik_n x}, \tag{2}$$

$$u^{(\mathrm{II})} = \sum_{\alpha=0}^{\infty} p_{\alpha m}\Psi_\alpha(y)e^{ik_\alpha x} + q_{\alpha m}\Psi_\alpha(y)e^{-ik_\alpha x}, \tag{3}$$

$$u^{(\mathrm{III})} = \sum_{n=0}^{\infty} t_{nm}\Psi_n(y)e^{ik_n x}, \tag{4}$$

where m, α, and n are the mode indices for waves in regions I, II, and III, respectively. r_{nm} and t_{nm} in Eqs. (2) and (4) are the reflection and transmission amplitudes which we wish to know. $p_{\alpha m}$ and $q_{\alpha m}$ in Eq. (3) are constants to be determined. $\Psi_m(y)$ and $\Psi_\alpha(y)$ are orthonormal transverse wave functions in terminal and the central T-shaped regions, respectively; $\Psi_{m/\alpha}(y)=\sqrt{\frac{2}{\mathbf{a/L}}}\cos\left(\frac{m/\alpha\pi y}{\mathbf{a/L}}\right)$. This is different from the case of electron wave propagation for which the boundary condition is $u=0$.[14] In the above equations, k_m, k_n, and k_α are the corresponding longitudinal wave vectors and satisfy the dispersion relation below:

$$\omega^2 = \omega_m^2 + v^2k_m^2 = \omega_n^2 + v^2k_n^2 = \omega_\alpha^2 + v^2k_\alpha^2, \tag{5}$$

in which $\omega_m=\frac{m\pi v}{\mathbf{a}}$, $\omega_n=\frac{n\pi v}{\mathbf{a}}$, and $\omega_\alpha=\frac{\alpha\pi v}{\mathbf{L}}$ are the cutoff frequencies of modes m, n, and α. Again, integers m,n, and α label the subbands of waves inside the wire. The velocity is assumed to be $v=5000\ \mathrm{m\ s^{-1}}$.

To calculate the coefficients r_{nm}, t_{nm}, $p_{\alpha m}$, and $q_{\alpha m}$, we match the waves at the boundaries of different regions. For phonon wave, the wave function and its derivative are continuous across the boundaries; therefore, we have

$$\sum_{\alpha=0}^{\infty}\Psi_\alpha(y)[p_{\alpha m}+q_{\alpha m}] = \Psi_m(y) + \sum_{n=0}^{\infty} r_{nm}\Psi_n(y), \quad 0 \leqslant y \leqslant \mathbf{a}, \tag{6}$$

$$\sum_{\alpha=0}^{\infty} ik_\alpha\Psi_\alpha(y)[p_{\alpha m}-q_{\alpha m}] = ik_m\Psi_m(y) - \sum_{n=0}^{\infty} ik_n r_{nm}\Psi_n(y), \quad 0 \leqslant y \leqslant \mathbf{a}, \tag{7}$$

$$\sum_{\alpha=0}^{\infty} \imath k_\alpha\Psi_\alpha(y)[p_{\alpha m}-q_{\alpha m}] = 0, \quad \mathbf{a} < y \leqslant \mathbf{L}, \tag{8}$$

$$\sum_{\alpha=0}^{\infty}\Psi_\alpha(y)[p_{\alpha m}e^{ik_\alpha b}+q_{\alpha m}e^{-ik_\alpha b}] = \sum_{n=0}^{\infty} t_{nm}\Psi_n(y)e^{ik_n b}, \quad 0 \leqslant y \leqslant \mathbf{a}, \tag{9}$$

$$\sum_{\alpha=0}^{\infty} ik_\alpha\Psi_\alpha(y)[p_{\alpha m}e^{ik_\alpha b}-q_{\alpha m}e^{-ik_\alpha b}] = \sum_{n=0}^{\infty} ik_n t_{nm}\Psi_n(y)e^{ik_n b}, \quad 0 \leqslant y \leqslant \mathbf{a}, \tag{10}$$

$$\sum_{\alpha=0}^{\infty} ik_\alpha\Psi_\alpha(y)[p_{\alpha m}e^{ik_\alpha b}-q_{\alpha m}e^{-ik_\alpha b}] = 0, \quad \mathbf{a} < y \leqslant \mathbf{L}. \tag{11}$$

Multiplying the transverse wave function $\Psi_n(y)$ in the two sides of Eqs. (6) and (9) and $\Psi_\alpha(y)$ in the two sides of Eqs. (7)–(11), after integrating these equations, we obtain

$$\delta_{nm} + r_{nm} = \sum_{\alpha=0}^{\infty} A_{n\alpha}[p_{\alpha m} + q_{\alpha m}], \tag{12}$$

$$k_m A_{m\alpha} - \sum_{n=0}^{\infty} k_n r_{nm} A_{n\alpha} = k_\alpha [p_{\alpha m} - q_{\alpha m}], \tag{13}$$

$$\tilde{t}_{nm} = \sum_{\alpha=0}^{\infty} A_{n\alpha}[p_{\alpha m} e^{ik_\alpha b} + q_{\alpha m} e^{-ik_\alpha b}], \tag{14}$$

$$\sum_{n=0}^{\infty} \tilde{t}_{nm} k_n A_{n\alpha} = k_\alpha [p_{\alpha m} e^{ik_\alpha b} - q_{\alpha m} e^{-ik_\alpha b}], \tag{15}$$

where $A_{n\alpha} = \int_0^a \Psi_n(y)\Psi_\alpha(y)dy$ and $\tilde{t}_{nm} = t_{nm} e^{ik_n b}$.

In terms of Eqs. (12)–(15), we get the following equations:

$$\sum_{l=0}^{\infty} \left[\sum_{\alpha=0}^{\infty} k_\alpha^{-1} k_l A_{l\alpha} A_{n\alpha} \frac{2}{e^{-ik_\alpha b} - e^{ik_\alpha b}} \right] r_{lm} + \sum_{l=0}^{\infty} \left[\delta_{\ln} + \sum_{\alpha=0}^{\infty} k_\alpha^{-1} k_l A_{l\alpha} A_{n\alpha} \frac{e^{-ik_\alpha b} + e^{ik_\alpha b}}{e^{-ik_\alpha b} - e^{ik_\alpha b}} \right] \tilde{t}_{lm} = \sum_{\alpha=0}^{\infty} k_\alpha^{-1} k_n A_{n\alpha} A_{m\alpha} \frac{2}{e^{-ik_\alpha b} - e^{ik_\alpha b}}, \tag{16}$$

$$\sum_{l=0}^{\infty} \left[\sum_{\alpha=0}^{\infty} k_\alpha^{-1} k_l A_{l\alpha} A_{n\alpha} \frac{e^{-ik_\alpha b} + e^{ik_\alpha b}}{e^{-ik_\alpha b} - e^{ik_\alpha b}} + \delta_{\ln} \right] r_{lm} + \sum_{l=0}^{\infty} \left[\sum_{\alpha=0}^{\infty} k_\alpha^{-1} k_l A_{l\alpha} A_{n\alpha} \frac{2}{e^{-ik_\alpha b} - e^{ik_\alpha b}} \right] \tilde{t}_{lm} = -\delta_{mn} + \sum_{\alpha=0}^{\infty} k_\alpha^{-1} k_m A_{n\alpha} A_{m\alpha} \frac{e^{-ik_\alpha b} + e^{ik_\alpha b}}{e^{-ik_\alpha b} - e^{ik_\alpha b}}. \tag{17}$$

Equations (16) and (17) are a set of linear equations for quantities $\tilde{t}_{lm}$ and r_{lm}, which can be solved by standard matrix inversion. Afterward, the transmission and reflection coefficients can be expressed as

$$\tilde{T}_m(\omega) = n \sum \tilde{T}_{nm}(\omega) = \sum_n \theta(\omega - \omega_n) |t_{nm}|^2 k_n / k_m, \tag{18}$$

$$R_m(\omega) = n \sum R_{nm}(\omega) = \sum_n \theta(\omega - \omega_n) |r_{nm}|^2 k_n / k_m, \tag{19}$$

where the function $\theta(\omega - \omega_n)$ is zero for $\omega < \omega_n$ and is unity for $\omega \geqslant \omega_n$. Its existence simply reflects the nature of a waveguide: when the frequency of the incoming wave $\omega < \omega_n$, in terms of the dispersion relation [Eq. (5)], the wave vector of the nth mode is imaginary so that mode cannot propagate. The transmission coefficient $\tilde{T}_m(\omega)$ represents the probability that phonons transmit into the outgoing terminal from the mth subband with total energy $\hbar\omega$ in the incoming terminal. Similarly, the reflection coefficient $R_m(\omega)$ represents the probability that phonons are reflected into the incoming terminal. Quantities $\tilde{T}_{nm}$ and R_{nm} represent the transmission coefficient and reflection coefficient between two single subbands, e.g., $\tilde{T}_{nm}$ gives transmission probability from subband m in the incoming terminal to subband n in the outgoing terminal. Clearly, due to time reversal invariance, if we exchange indices $m \leftrightarrow n$, the transmission coefficient does not change.

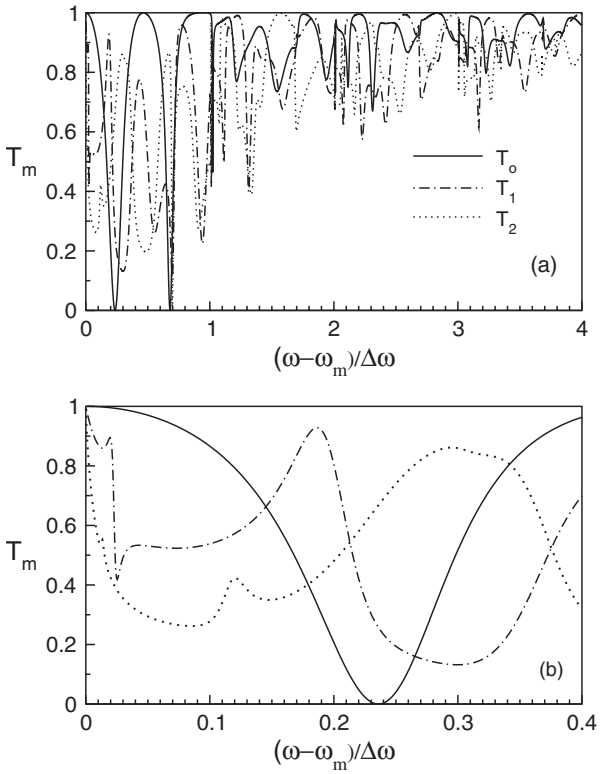

FIG. 2. [(a) and (b)] Transmission coefficient $T_m(\omega)$ vs the incident frequency ω for the geometrical parameters $a=10$ nm, $b=10$ nm, and $L=30$ nm. ω_m is the mth mode cutoff frequency. The horizontal axis is scaled by $\Delta\omega \equiv \omega_{m+1} - \omega_m = \frac{\pi v}{a}$, where the velocity is fixed at $v=5000$ m/s.

III. FEATURES OF TRANSMISSION COEFFICIENTS

Figure 2 plots the transmission coefficient $\tilde{T}_m(\omega)$ versus frequency $(\omega - \omega_m)$ for different lengths L of the side stub in the T-shaped junction where we fixed the wire width **a** and side-stub width **b**. Here, ω_m is the cutoff of the mth vibrational mode in the incoming terminal wire. All the transmission coefficients exhibit strong oscillations versus phonon energy $\hbar\omega$. $\tilde{T}_m$ can reach unity for certain frequencies (energies), showing a clear resonance transmission behavior. For the Zeroth mode, $\tilde{T}_0$ can dip to zero indicating antiresonances where total reflection occurs. $\tilde{T}_0$ also shows a good quasiperiodic variation versus energy $\hbar\omega$. Similar quasiperiodic behavior was reported for electron transport in T-shaped junctions.[16,17] The behavior of other modes is much more irregular, in particular, $\tilde{T} \neq 0$ for all $m > 0$. The oscillation amplitude becomes smaller as ω increases, and $\tilde{T}_m$ ap-

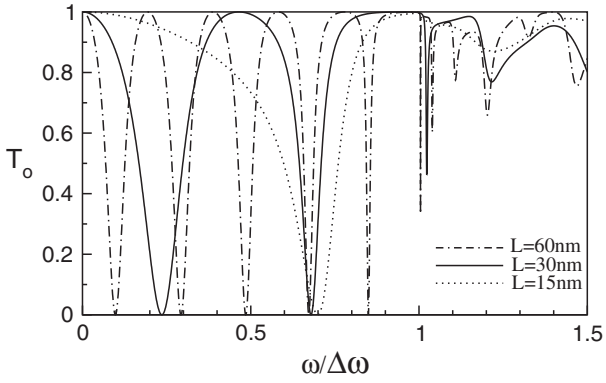

FIG. 3. Transmission coefficient $T_0(\omega)$ vs the incident phonon frequency ω with different stub lengths L. Other parameters are same as those in Fig. 2.

proaches unity for large ω because high energy phonons can easily traverse from left lead to the right lead via the side-stub region (region II, see Fig. 1).

In Fig. 2, we observe that the $m=0$ mode shows a quasi-periodic characteristic in the frequency range $(\omega-\omega_m)/\Delta\omega<1$ [where $\Delta\omega=(\omega_{m+1}-\omega_m)$ is the difference of frequencies between neighboring modes], while it becomes rather irregular for higher frequencies. This behavior is shown more clearly in Fig. 3. This shows that $\tilde{T}_0(\omega)$ consists of two behaviors: periodicity and nonperiodicity. In the periodic part, the period of the oscillation reduces when the stub length L increases. In the nonperiodic part, transmission coefficient has an irregular oscillation. We now investigate these behavior in more detail.

The periodic behavior of $\tilde{T}_0(\omega)$ at $\omega/\Delta\omega<1$ can be understood as the result of wave interference. For this small range of incoming phonon energy, the outgoing phonons must also stay at the massless mode. Then, when the incoming wave enters the stub region from left lead, it can excite modes inside the stub with indices $\alpha>0$ because the stub length L is wider than the wire width [by Eq. (5), the wider the width, the closer the modes]. These different modes will interfere with one another and cause a periodic behavior of $\tilde{T}_0(\omega)$. Afterward, the waves will exit to the massless mode of the right lead. When L is increased further, the mode spacing of the stub region becomes smaller, and more modes will be excited by the incoming wave, thereby reducing the transmission periodicity. The period of the oscillation can be roughly estimated as $\mathbf{a}/(\mathbf{L}-\mathbf{a})$.

When energy of the incoming phonons is large, i.e., when $\omega/\Delta\omega>1$, in the outgoing lead, the modes with $m>0$ can be excited. In other words, although the incoming mode is massless, the outgoing modes can be "massive" $(m>0)$. This causes transmission coefficient $\tilde{T}_0(\omega)$ to lose the regular periodic feature, as shown in Figs. 2 and 3. Indeed, when more modes are excited in the right lead, according to Eq. (18), $\tilde{T}_0(\omega)$ is a summation of many terms $\tilde{T}_{00}(\omega)$, $\tilde{T}_{10}(\omega)$,.... Adding many oscillatory functions results in the irregular behavior.

So far, we have discussed the periodic features of transmission coefficient with frequency. It turns out that there is a

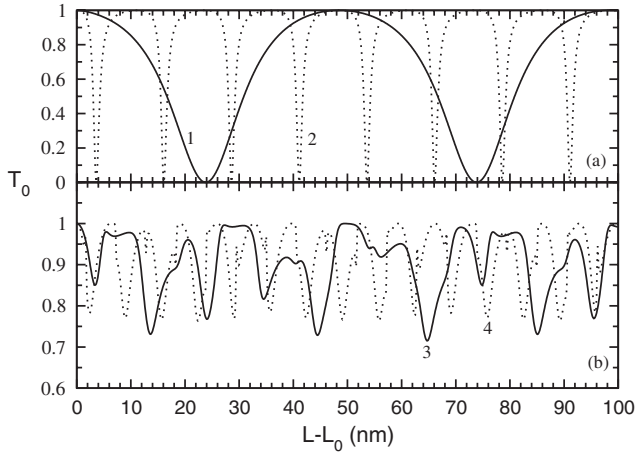

FIG. 4. Transmission coefficient $T_0(\omega)$ vs stub length L with fixed incident frequencies. $L_0=10$ nm. (a) $\omega=\frac{\pi v}{5a}$ for curve 1 and $\omega=\frac{4\pi v}{5a}$ for curve 2; (b) $\omega=\frac{7\pi v}{5a}$ for curve 3 and $\omega=\frac{9\pi v}{5a}$ for curve 4. Other parameters are same as those in Fig. 2.

periodic behavior against the stub length $\mathbf{L}$ as well. Such a behavior shows even clearer the wave interference phenomenon. For our example system, Fig. 4(a) plots $\tilde{T}_0$ versus $\mathbf{L}$ for four fixed frequencies below the first cutoff frequency. A very reasonable periodic behavior is clearly seen. When ω increases, the period of the oscillation decreases. Examining Fig. 4(a), it is evident that the period in $\tilde{T}(L)$ is roughly π/k, where $k=\omega/v$. This clear periodic behavior is due to interference. When the incoming wave enters the stub region, it partly goes into the stub and gets reflected back at the far end of the stub. This reflected wave interferes with the incoming wave coherently, producing the periodic change of $\tilde{T}_0$ as $\mathbf{L}$ is increased. Finally, in Fig. 4(b), we plot waves with frequencies higher than the first cutoff, where $\tilde{T}(L)$ loses the periodic feature. This is, again, due to the summation of the mode-to-mode transmission coefficients as discussed above.

IV. THERMAL CONDUCTANCE

So far, we have discussed the transmission coefficient properties in the T-shaped dielectric junction. In this section, based on the above results, we investigate thermal conductance in the T-shaped junction. The formula of thermal flux by which the energy flux $\dot{Q}$ is from the left lead to the right lead can be expressed as[1,2,7,23]

$$\dot{Q}=\sum_m \int_{\omega_m}^{\infty} \frac{d\omega}{2\pi}\hbar\omega[\eta_L(\omega)-\eta_R(\omega)]\tilde{T}_m(\omega), \qquad (20)$$

where $\eta_{(L/R)}(\omega)$ is the Bose-Einstein distribution function of the phonons in the left/right reservoir, and ω_m is the cutoff frequency for the mode m in the leads. In the following, we assume that the temperature difference $\Delta T=T_L-T_R$ is very small; therefore, the thermal conductance can be obtained straightforwardly from Eq. (20):

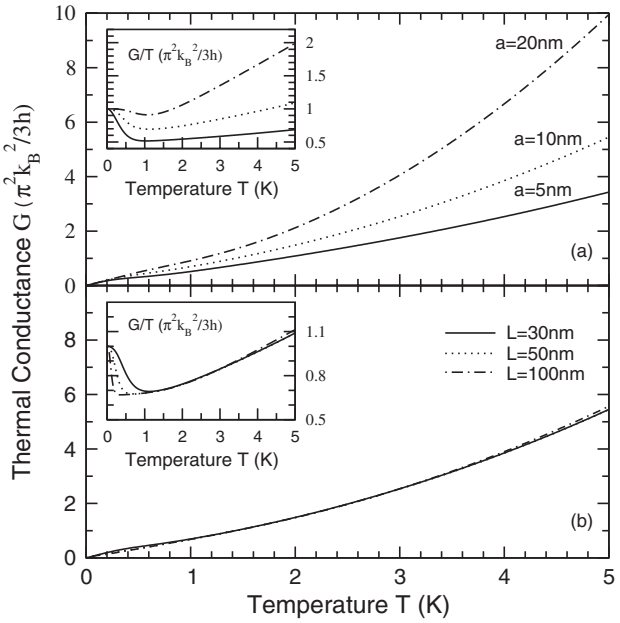

FIG. 5. Thermal conductance G (main plot) and G/T (inset) vs temperature T. (a) For different widths of wire. (b) For different lengths of stub. Other parameters are same as those in Fig. 2.

$$G = \lim_{\Delta T \to 0} \frac{\dot{Q}}{\Delta T} = \sum_m \int_{\omega_m}^{\infty} \frac{d\omega}{2\pi} \hbar\omega \tilde{T}_m(\omega) \frac{d\eta(\omega)}{dT}. \quad (21)$$

In terms of Eq. (21), we will study and discuss thermal conductance under the influence of external factors, e.g., temperature and geometrical structure. We emphasize that Eq. (21) is a general result for any two-probe dielectric system. First, we consider how does thermal conductance G change with temperature T. Since $d^2\eta(\omega)/dT^2 > 0$ for any ω and T, and $\tilde{T}_m(\omega)$ must certainly be non-negative, we conclude from Eq. (21) that $dG(T)/dT \geq 0$. This means that the thermal conductance must be a monotonically increasing function of temperature for any two-probe devices. For our T-shaped junction example, Fig. 5 confirms this behavior. Although the transmission coefficient $\tilde{T}_m(\omega)$ has many oscillations as we presented in the previous section, these oscillations do not appear in thermal conductance. This is because the wide energy integration range in Eq. (21) smears out the oscillations in $\tilde{T}_m(\omega)$. It is also worth noting that this monotonic behavior is different from that of the electric conductance, which does not have to change monotonically with both temperature and bias voltage.[21,22]

Numerically, Fig. 5 plots G as a function of temperature T for the T-shaped junction, for a fixed stub width $\mathbf{b}=10$ nm and several values of stub length $\mathbf{L}$ as well as terminal width $\mathbf{a}$. At higher temperatures, e.g., $T>2$ K, the thermal conductance G is proportional to T^2. At low temperatures, e.g., $T<0.1$ K, G is a linear function of T. These results are similar to those of previous works on two-probe devices.[4] In certain temperature range, e.g., near $T\sim 0.5$ K, G versus T may exhibit a $T^{1/x}$ behavior ($x>1$), where G increases very slowly with temperature. The change of stub length $\mathbf{L}$ has some

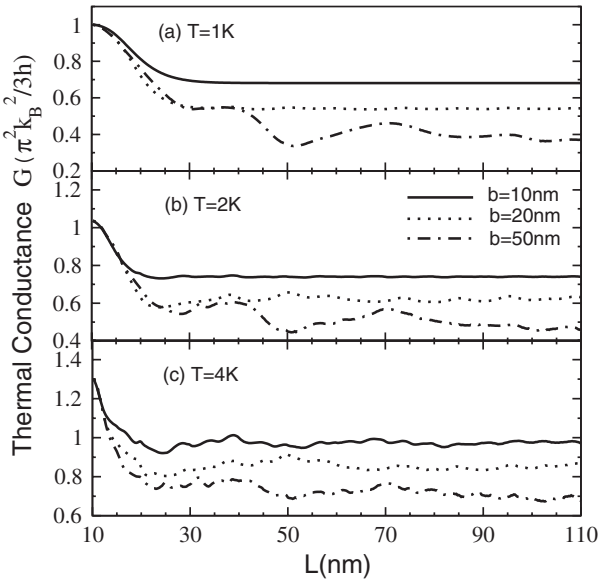

FIG. 6. Thermal conductance G vs the stub length with different widths $b=10$, 20, and 50 nm. Temperature is (a) 1 K, (b) 2 K, and (c) 4 K. Other parameters are the same as those in Fig. 2.

effect on G in the range $T<1$ K, as shown in Fig. 5(b), but this effect diminishes for $T>1$ K. As discussed previously, when $T<1$ K, only the massless phonon mode can propagate in the lead of the T-shaped wire. The change of $\mathbf{L}$ causes transmission coefficient to vary periodically for $\omega < \Delta\omega$, as seen in Fig. 4(a). Perhaps this has led to the slight change in G. When $T>1$ K, although an irregular behavior appears in the transmission coefficients (see last section), G has little change when $\mathbf{L}$ is varied. Again, it is confirmed that the wide energy range involved in thermal conductance calculation smears out all oscillations in the transmission coefficient.

Can we observe the universal quantum, $G_0 \equiv \pi^2 k_B^2 T/3$ h, of thermal conductance in the T-shaped junction? To see this, we plot G/T versus temperature T in the inset in Fig. 5 for several values of $\mathbf{a}$ and $\mathbf{L}$. We found that G/T exhibits a nonmonotonic behavior and has a minimum at $T \neq 0$. Similar behavior has been observed in the experiments of Schwab *et al.*[8] Importantly, in the zero temperature limit, our calculation of G/T, for all values of $\mathbf{L}$, tends to unity in terms of the universal quantum G_0, as Fig. 5 shows. For such a low temperature, only the zeroth mode is open for transport, and one can easily confirm that the occupation number for the first mode at $T=0.1$ K is merely $\eta(\omega_{cut}) \sim 0$ (again, $\omega_{cut} = \frac{\pi v}{\mathbf{a}}$). Hence, only the massless mode whose transmission coefficient $\tilde{T}_0 \sim 1$ contributes to G. The transport is therefore in the universal regime as our calculation shows. The universal quantum obtained at $T \to 0$ limit is also independent of other device parameters: width $\mathbf{b}$ of the stub and width $\mathbf{a}$ of leads. Figure 5 shows G and G/T versus T for different $\mathbf{a}$'s and different $\mathbf{L}$'s. It is obvious that at low temperature, $G = \pi^2 k_B^2 T/3$ h so that $G/T = \pi^2 k_B^2/3$ h, for all the cases. Clearly, the thermal conductance G increases with $\mathbf{a}$: a wider wire transports more energy.

Finally, we plot G versus stub length $\mathbf{L}$ for the T-shaped junction for three stub widths $\mathbf{b}$ in Fig. 6. At 1 K, when $\mathbf{L}$ is

equal to the wire width **a**, i.e., no stub at all (see Fig. 1), transmission coefficient $\tilde{T}_m(\omega)=1$ for all m and G reaches its maximum value G_0. G reduces for $\mathbf{L}>\mathbf{a}$ due to wave scattering and has lower values for larger **b**'s. This is because geometrical size increasing means that scattering region becomes larger so that the stronger scattering happens. It is also found that at $T>1$ K, G with $\mathbf{L}=\mathbf{a}$ is larger than the universal value due to the contribution from massive modes in addition to the massless mode, as discussed above.

V. CONCLUSIONS

We have investigated phonon transmission properties and thermal conductance for a T-shaped dielectric wire by a mode matching numerical technique. Due to quantum interference, transmission coefficients of phonons become quite complicated. $\tilde{T}_m(\omega)$ has an oscillation behavior with quasiperiodicity and irregularity. For the thermal conductance of such a system, we deduced that it increases monotonically with the temperature—a result that is generally true for any two-probe device. We confirmed the existence of universal quantum of thermal conductance which exists at the low temperature limit, and such a quantum is robust against all the system parameters.

ACKNOWLEDGMENTS

This work was supported in part by grants provided by the Hong Kong Research Grants Council (RGC) and the Hong Kong Baptist University Faculty Research Grant (FRG) and in part by grants provided by the NSERC of Canada and FCAR of Québec.

[1] L. G. C. Rego and G. Kirczenow, Phys. Rev. Lett. **81**, 232 (1998).
[2] M. P. Blencowe, Phys. Rev. B **59**, 4992 (1999).
[3] B. A. Glavin, Phys. Rev. Lett. **86**, 4318 (2001).
[4] A. Kambili, G. Fagas, Vladimir I. Fal'ko, and C. J. Lambert, Phys. Rev. B **60**, 15593 (1999).
[5] A. Ozpineci and S. Ciraci, Phys. Rev. B **63**, 125415 (2001).
[6] D. H. Santamore and M. C. Cross, Phys. Rev. Lett. **87**, 115502 (2001); Phys. Rev. B **63**, 184306 (2001).
[7] D. E. Angelescu, M. C. Cross, and M. L. Roukes, Superlattices Microstruct. **23**, 673 (1998).
[8] K. Schwab, E. A. Henriksen, J. M. Worlock, and M. L. Roules, Nature (London) **404**, 974 (2000).
[9] T. S. Tighe, J. M. Worlock, and M. L. Roukes, Appl. Phys. Lett. **70**, 2687 (1997).
[10] M. M. Leivo and J. P. Pekda, Appl. Phys. Lett. **72**, 1305 (1998).
[11] W. Holmes, J. M. Gildemeister, and P. L. Richards, Appl. Phys. Lett. **72**, 2250 (1998).
[12] R. Landauer, IBM J. Res. Dev. **1**, 223 (1957); Philos. Mag. **21**, 863 (1970).
[13] Q.-F. Sun, P. Yang, and H. Guo, Phys. Rev. Lett. **89**, 175901 (2002).
[14] A. Szafer and A. D. Stone, Phys. Rev. Lett. **62**, 300 (1989).
[15] J. Wang, H. Guo, and R. Harris, Appl. Phys. Lett. **59**, 3075 (1991); J. Wang and H. Guo, *ibid.* **60**, 654 (1992).
[16] H. Wu, D. W. L. Sprung, J. Martorell, and S. Klarsfeld, Phys. Rev. B **44**, 6351 (1991).
[17] F. Sols, M. Macucci, U. Ravaioli, and K. Hess, Appl. Phys. Lett. **54**, 350 (1989); J. Appl. Phys. **66**, 3892 (1989).
[18] E. V. Bezuglyi and V. Vinokur, Phys. Rev. Lett. **91**, 137002 (2003).
[19] S.-X. Qu and M. R. Geller, Phys. Rev. B **70**, 085414 (2004).
[20] Y. Meir, N. S. Wingreen, and P. A. Lee, Phys. Rev. Lett. **66**, 3048 (1991).
[21] H.-Q. Xu, Phys. Rev. B **50**, 8469 (1994).
[22] B. A. Auld, *Acoustic Field and Waves in Solid* (Krieger, Malabar, FL, 1990).
[23] M. Büttiker, IBM J. Res. Dev. **32**, 63 (1988); Phys. Rev. B **38**, 9375 (1988).